

Analytical and Finite Element Methods for Evaluative Electromagnetic Parameters of Inset PMSM and SPMSM



Phi Do Chi¹, Hoang Bui Huu², Vuong Dang Quoc³, Dinh Bui Minh^{3*}

¹ Electrical-Electronic Engineering, Cao Thang Technical College, Ho Chi Minh City 700000, Vietnam

² Faculty of Electrical Engineering - Automation, University of Economics, Technology for Industries, Ha Noi City 100000, Viet Nam

³ School of Electrical and Electronic Engineering, Hanoi University of Science and Technology, Ha Noi City 100000, Viet Nam

Corresponding Author Email: dinh.buiminh@hust.edu.vn

Copyright: ©2025 The authors. This article is published by IETA and is licensed under the CC BY 4.0 license (<http://creativecommons.org/licenses/by/4.0/>).

<https://doi.org/10.18280/jesa.580214>

ABSTRACT

Received: 8 January 2025

Revised: 11 February 2025

Accepted: 18 February 2025

Available online: 28 February 2025

Keywords:

permanent magnet synchronous motor (SPMSM), interior permanent magnet synchronous (IPMSM), back electromotive force (EMF), torque ripple, analytical model, finite element analysis

Permanent magnet synchronous motors (PMSMs) are widely used in the fields of electric vehicles (EVs) industry due to their remarkable power density, lightweight design, remarkable efficiency, and low torque inertia. Surface-mounted PMSM (SPMSM) and inset PMSM are the two types of PMSMs that can be distinguished by the location of the permanent magnet (PM) in the rotor. This paper presents an association of the analytical model and finite element method (FEM) for evaluative electromagnetic parameters for the SPMSM and inset PMSM. The approach is here performed in two steps: First, an analytical model is presented for both motors to determine initial parameters, including stator dimensions, rotor dimensions, and PM properties. And then, the FEM is proposed to evaluate performance characteristics of the two proposed motors, such as magnetic fields, torque ripple, cogging torque, electromagnetic torque and back electromotive force. The simulation results highlight the performance differences between the two motor types.

1. INTRODUCTION

Permanent magnet synchronous motors (PMSMs), particularly surface-mounted (SPMSMs), are widely used in the fields of electric vehicles (EVs) industry due to advancements in industrialization and technology [1, 2]. In the study [3], the study highlighted the benefits of outer rotor PMSMs through two approaches: comparing torque capabilities of two hypothetical permanent magnet (PM) configurations based on their geometric volumes and evaluating their performance. In the study [4], the torque characteristics of proposed geometries were analyzed via the finite element method (FEM) with a nonlinear model. In the studies [5-7], the papers also conducted comprehensive analyses of interior PMSMs (IPMSMs) and SPMSMs with various slot and pole configurations. These studies utilized quantitative models to compare back electromotive force (EMF), torque ripple, cogging torque, total harmonic distortions (THDs), and loss characteristics. An optimized design for IPMSMs was developed to define key dimensions, followed by the FEM simulations to reduce cogging torque and enhance efficiency [8]. The FEM was proposed for SPMSMs with inner and outer rotor configurations to compare the flux density of the PM [9]. It found that while outer rotor designs produced significantly higher torque, they also exhibited higher cogging torque. Feng et al. [10] reviewed the use of SPMSMs in diverse applications such as electric drives, marine propulsion, lifting systems, and mining due to their

compact size, high torque at low speeds, efficiency, and superior performance, especially with rare-earth magnet developments. In the study [11], the SPMSMs were further classified into inner and outer rotor types based on rotor positioning. In the study [12], the separate models of IPMSMs with different multilayer PM configurations were analyzed, revealing enhanced performance with double-layer PMs. Du et al. [13] focused on analysing the cogging torque distribution in PM machines via the slot and pole combinations. In the studies [14, 15], comprehensive assessments of the SPMSMs and IPMSMs from a multi-physics perspective were presented to study the optimized design for the practical machine with the output power of 60 kW and speed of 30,000 rpm. Arehpanahi and Kheiry [16] evaluated the suitability of SPMSMs and IPMSMs for high-speed applications by comparing their electromagnetic properties and demagnetization behaviors using the FEM. The conclusion was that although IPMSMs provide better cost-effectiveness and torque per permanent magnet weight, their rotor structures are less durable and more susceptible to irreversible demagnetization. Finally, Xuan [17] also used the FEM to compare four distinct rotor structures of PMSMs with the high-speed. This study evaluated the stress levels, temperature rise and sleeve thickness under various conditions.

Although there have been numerous studies on SPMSMs as mentioned above, but the combination of analytical and numerical methods to analyze and evaluate the two types of SPMSMs and inset SPMSMs with inner rotor configuration

has not been addressed in previous research. In this contribution, comparative electromagnetic parameters of the SPMSM and inset PMSM are proposed via the association between the analytical model and FEM. The approach is here presented in two steps: An analytical model is first presented to design initial dimensions of both motors (including stator dimensions, rotor dimensions, and PM properties). Next, the FEM is conducted to evaluate and simulate electromagnetic parameters of the practical motors, such as magnetic fields, torque ripple, cogging torque, electromagnetic torque, and back electromotive force (EMF). The simulation results will show the highlight of advantages and disadvantages of two motor types.

2. ANALYTICAL COMPUTATION

This part highlights magnetic and electric properties that influence the sizing and selection of key parameters in the machine's design. A theoretical framework is employed to develop an analytical model that defines the machine's dimensions. One critical parameter in designing the PMSM is the fundamental flux density in the air gap (B_δ). This parameter directly determines the size of the PM in the PMSM, including its thickness (h_m) and coverage angle (2α). Assuming the flux density distribution over the magnets (B_m) is rectangular, as illustrated in the study [18], and neglecting flux leakage, the expression for B_δ is derived as follows:

$$B_\delta = \frac{4}{\pi} B_{r,m} \sin\alpha \quad (1)$$

where, α is defined in electrical degrees. The flux density above the magnets (B_m) can be defined via the remanence flux of PM ($B_{r,m}$) as follows [19]:

$$B_{r,m} = B_{r,o} \cdot [1 - T_k \cdot (T_r - T_o)] \cdot \frac{1}{1 + \mu_{r,m} \frac{\delta_g}{h_m}} \quad (2)$$

where, δ_g represents the equivalent air gap length, $\mu_{r,m}$ is the relative permeability of the PM, $B_{r,o}$ is the PM remanent density at the ambient temperature ($T_o=20^\circ\text{C}$), T_r is the PM working temperature ($T_r=30^\circ\text{C}$) [19], T_k is the temperature coefficient of PM [$1/^\circ\text{C}$] ($T_k=0,001$) [19] and h_m is the thickness of the PM.

By taking into account Eqs. (1) and (2), one gets:

$$h_m = \frac{\mu_r \delta_g}{\frac{B_{r,o} \cdot [1 - T_k \cdot (T_r - T_o)] \cdot 4 \sin\alpha}{B_g \pi} - 1} \quad (3)$$

In general, the δ_g for the PMSM machines is selected from 1 mm to 3 mm. The selection of δ_g depends on various characteristics influenced by the air gap length (g) [18, 19].

The inner diameter of the stator (D_{is}) is defined as:

$$D_{is} = \left(\frac{V_r \times 4}{\pi \times k_{shape}} \right)^{\frac{1}{3}} \quad (4)$$

where, k_{shape} is the shape factor that can be selected from 2 to 3 [18], and V_r is the volume of the rotor determined via the electromagnetic torque (T) and the torque density (TRV) [18].

From the Eqs. (3) and (4), the PM width (w_m) is defined as [20]:

$$w_m = \frac{2\alpha \cdot \pi (D_{is} - 2g - 2h_m)}{180 \cdot p} \quad (5)$$

From the Eq. (2) to Eq. (5), the PM magnetic flux (ϕ_m) can be determined as:

$$\phi_m = B_m \cdot L \cdot w_m \quad (6a)$$

$$L = \frac{D_{is}}{k_{shape}} \quad (6b)$$

The distribution of fringing and leakage fluxes is assumed as in Figure 1 [20].

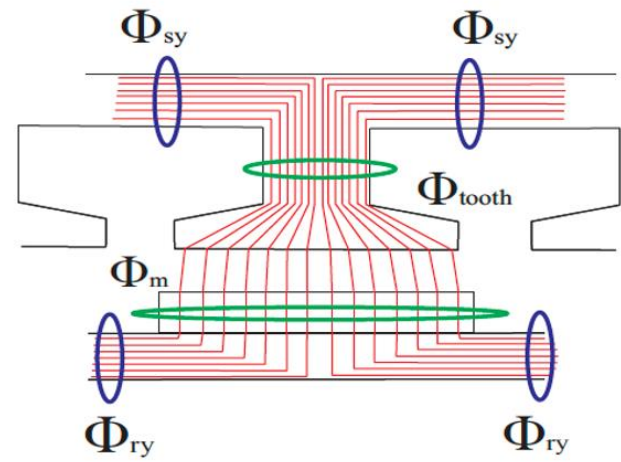


Figure 1. Flux lines of magnetic field through the stator and rotor [20]

Based on the Eq. (6a), the ϕ_m can be rewritten as:

$$\phi_m = 2\phi_{sy} = 2\phi_{ry} = \frac{Q}{2p} \cdot \phi_{tooth} \quad (7)$$

where, ϕ_{sy} , ϕ_{ry} , and ϕ_{tooth} are respectively the stator, rotor and tooth fluxes.

The height of stator yoke (h_{sy}) and rotor yoke (h_{ry}) are then defined as [20]:

$$h_{sy} = \frac{\phi_m}{2 \cdot B_{sy} \cdot L \cdot k_j}, \quad h_{ry} = \frac{\phi_m}{2 \cdot B_{ry} \cdot L \cdot k_j} \quad (8)$$

where, k_j is the pressed factor of the stator ($k_j=0,96$ defined in [20]), L is the length of stator. The tooth width is determined as [18-20]:

$$w_t = \frac{\phi_{tooth}}{B_t \cdot L \cdot k_j} \quad (9)$$

The turn number (N) on each tooth can be computed via the expression:

$$N = \frac{1.1 \cdot U_p}{2\sqrt{2} \cdot f \cdot q \cdot k_w \cdot B_{g,pk} \cdot D_{is} \cdot L} \quad (10)$$

where, U_p is the phase voltage, f is the frequency, q is the slot number per phase per pole, k_w is the concentrated winding factor defined in the study [20], and $B_{g,pk}$ is maximum flux density.

Finally, the stator slot open (b_2) is defined as [21]:

$$b_2 = \sqrt{b_1^2 - \frac{4\pi \times A_{slot}}{Q}} \quad (11)$$

where, A_{slot} is the slot area defined via the winding cross-section in each slot, b_1 is the bottom width of stator slot and Q is the slot number.

3. FINITE ELEMENT ANALYSIS

The Maxwell's equations in the frequency domain are written as [21-24]:

$$\text{curl } H = J_s \quad (12)$$

$$\text{curl } E = -j\omega B \quad (13)$$

$$\text{div } B = 0 \quad (14)$$

where, H , J_s , E , and B are the local magnetic field intensity (A/m), electric current density (A/m²), electric field (V/m) and local magnetic flux density (T).

The set of Maxwell's equations from Eqs. (10) to (12) is solved with the association of the boundary conditions and behavior laws, i.e.,

$$n \times H|_{\partial\Omega} = 0, B = \mu H, J = \sigma E \quad (15)$$

where, μ is the permeability (H/m), σ is the electrical conductivity (S/m) and J is the eddy current (A/mm²).

Based on the set of equations, from Eqs. (10) to (12), the A-conformal weak formulation can be written as:

$$(\mu^{-1} \text{curl } A \cdot \text{curl } A')_{\Omega} + (\sigma A \cdot A')_{\Omega_c} + j\omega (\sigma \text{grad } \varphi \cdot A')_{\Omega_c} + \langle n \times H \cdot A' \rangle_{\Gamma_h} = (J_s \cdot A')_{\Omega_s}, A' \in H_h^0(\text{curl}; \Omega) \quad (16)$$

where, Ω_c and Ω_s are, respectively, the conducting and inductor domains, Ω is the studied domain (with $\partial\Omega = \Gamma = \Gamma_h \cup \Gamma_c$) and A' is the test function. It should be noted that the fields of H , B , E , and J belong to the function space $H_h^0(\text{curl}; \Omega)$.

By solving the weak form of Eq. (16), the back EMF can be defined via the post-processing, i.e., [18]:

$$E = \frac{L}{S} \frac{\partial}{\partial t} \left(\iint_{\Omega^+} A d\Omega^+ - \iint_{\Omega^-} A d\Omega^- \right) \quad (17)$$

where, L and S are the length and cross-section area of the conductor.

4. SIMULATION TEST

In the first step, the practical SPMSM and inset PMSM of 7.5kW are considered. The initial parameters of two these

machines are given in Table 1. The analytical results of the two proposed machines are presented in Table 2.

Table 1. Initial parameters of two proposed motors

Parameters	SPMSM	Inset PMSM
Rated power (kW)	7.5	7.5
Rated voltage (V)	500	500
Frequency (Hz)	50	50
Efficiency (%)	93	93
Power factor	0.9	0.9
Phase number	3	3
Pole numbers	8	8

Table 2. Analytical results

Main Dimensions	SPMSM	Inset PMSM
Outer stator diameter (D_{os}) (mm)	224.42	224.42
Outer rotor diameter (D_{or}) (mm)	143.6	145.6
Inner stator diameter (D_{is}) (mm)	151.6	151.6
Rotor length (L_r) (mm)	151.6	151.6
Shaft rotor diameter (mm)	118	120
Stator slot (Q)	12	12
PM thickness (d_m) (mm)	3	3
Air gap thickness (g) (mm)	1	1

In the next step, the given analytical results are validated by using the FEM to determine the magnetic field density, cogging torque, torque ripple, back EMF, electromagnetic torque, harmonic components, flux linkage and temperature rise. The 2D geometry of the SPMSM and inset PMSM is depicted in Figure 2, while the flux density distributions for both motor types are pointed out in Figure 3. For the SPMSM, the maximum flux density is observed to be 2.120 T, compared to 2.097 T for the inset PMSM. This means that the flux density in the teeth of the inset PMSM is slightly smaller than that of the SPMSM.

Figure 4 highlights the back EMF of both motors, revealing smooth and sinusoidal waveforms. Minimal higher harmonic components, specifically the 11th and 13th, are present, as shown in Figure 5.

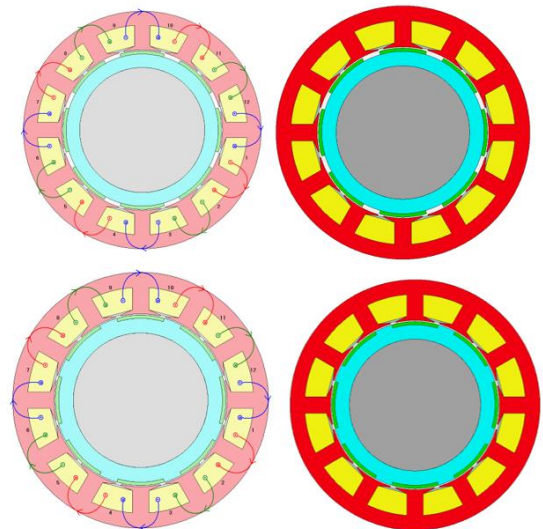


Figure 2. Modelling of SPMSM (top) and inset PM (bottom)

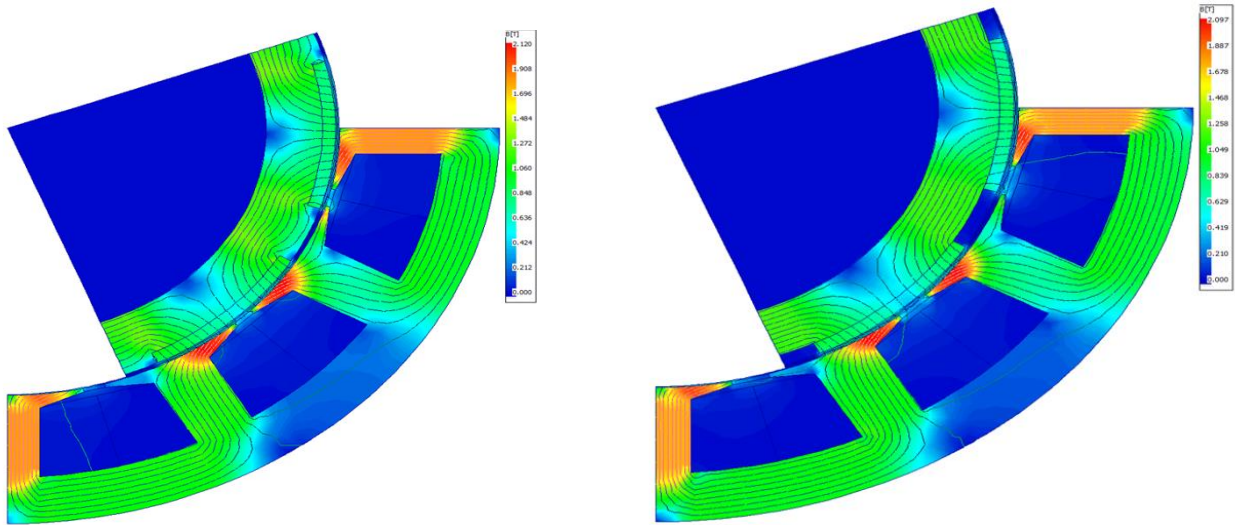


Figure 3. Flux density distribution of SPMSM (left) and inset PMSM (right)

The electromagnetic torque for the SPMSM and inset PMSM is illustrated in Figure 6. The SPMSM produces an average torque of 96.753 Nm, while the inset PMSM generates an average torque of 96.352 Nm. However, the inset PMSM demonstrates a slightly higher torque than the SPMSM, which is attributed to its larger rotor size. Figure 7 presents the cogging torque distributions. The SPMSM exhibits an average cogging torque of 19.703 Nm, which is 3.547 Nm lower than that of the inset PMSM. This reduction in cogging torque is due to the smaller teeth of the SPMSM. Consequently, the SPMSM is expected to offer better stability compared to the inset PMSM.

The torque ripple of the SPMSM and inset PMSM is shown in Figure 8. The torque ripple of the inset PMSM is smaller than that of the SPMSM.

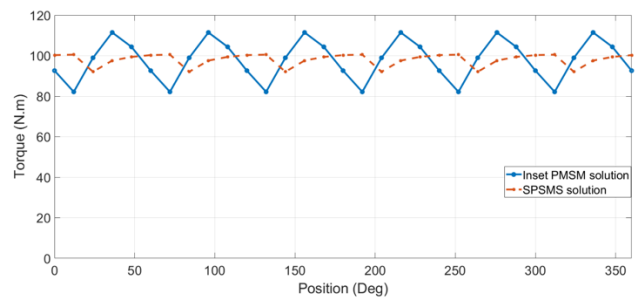


Figure 6. Electromagnetic torque of SPMSM and inset PMSM

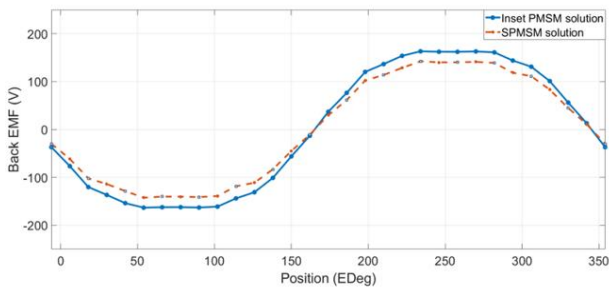


Figure 4. Back EMF distribution of SPMSM and inset PMSM

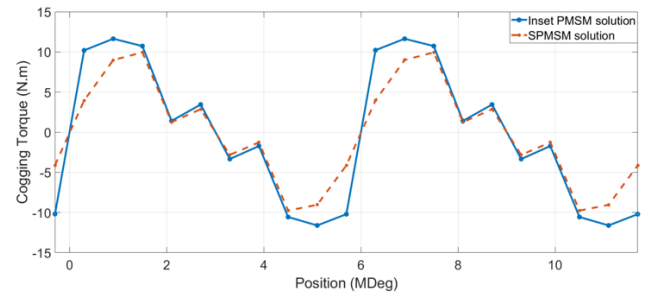


Figure 7. Cogging torque of SPMSM and inset PMSM

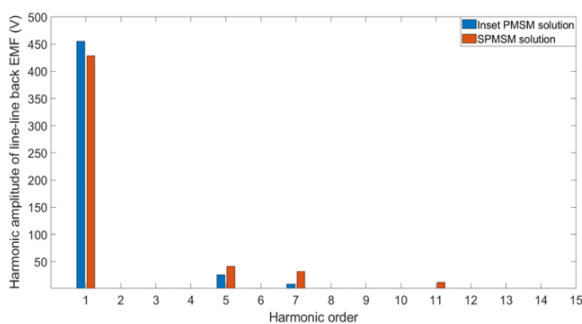


Figure 5. Harmonic components (THD) of Back EMF of two motors

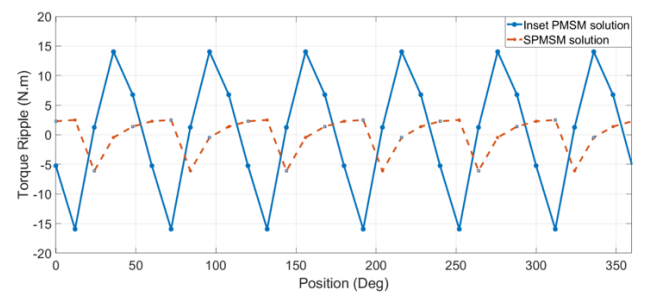


Figure 8. Torque ripple distribution of two proposed machines

The comparison of the flux linkages of the two proposed motors is pointed out in Figure 9. It can be seen that the waveforms and mean values for the inset PMSM are slightly greater than those of the SPMSM. Table 3 summarizes the key

parameters of the SPMSM and inset PMSM. Notably, the efficiency of the SPMSM is higher, at 93.95%, compared to 93.55% for the inset PMSM, with THD <3.5% for both cases. Based on the obtained results, it is important to emphasize the real-world consequences, especially in motor selection for different applications. When selecting between SPMSM and Inset PMSM, even small differences in efficiency could influence the choice in energy-sensitive applications, like electric vehicles, where maximizing range is crucial.

Table 3. Simulated results

Parameters	SPMSM	Inset PMSM	Unit
Efficiency	93.949	93.554	%
Output torque	96.753	96.352	Nm
Torque ripple	8.9508	30.022	%
Power factor	0.93587	0.84755	
Output Power	7599	7567.4	W
Total Losses	489.45	521.4	W

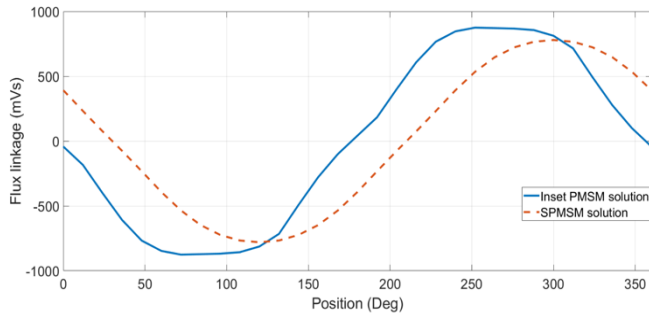


Figure 9. Flux linkage of SPMSM and inset PMSM

This indicates that the inset PMSM faces greater challenges in heat dissipation due to the placement of its permanent magnets. Additionally, the SPMSM has a larger rotor compared to the inset PMSM, which slightly increases its mean torque. The thermal performance of the inset PMSM is analyzed in Figure 10, where the temperature distribution is depicted using various colors. Figure 11 and Table 4 provide the temperature rise data at different positions for both the SPMSM and inset PMSM. The results indicate that the inset PMSM experiences higher temperatures than the SPMSM at all measured positions. For instance, the temperature at the stator slot of the SPMSM is approximately 0.5°C lower than that of the inset PMSM, and the temperature at the PM is 0.1°C lower.

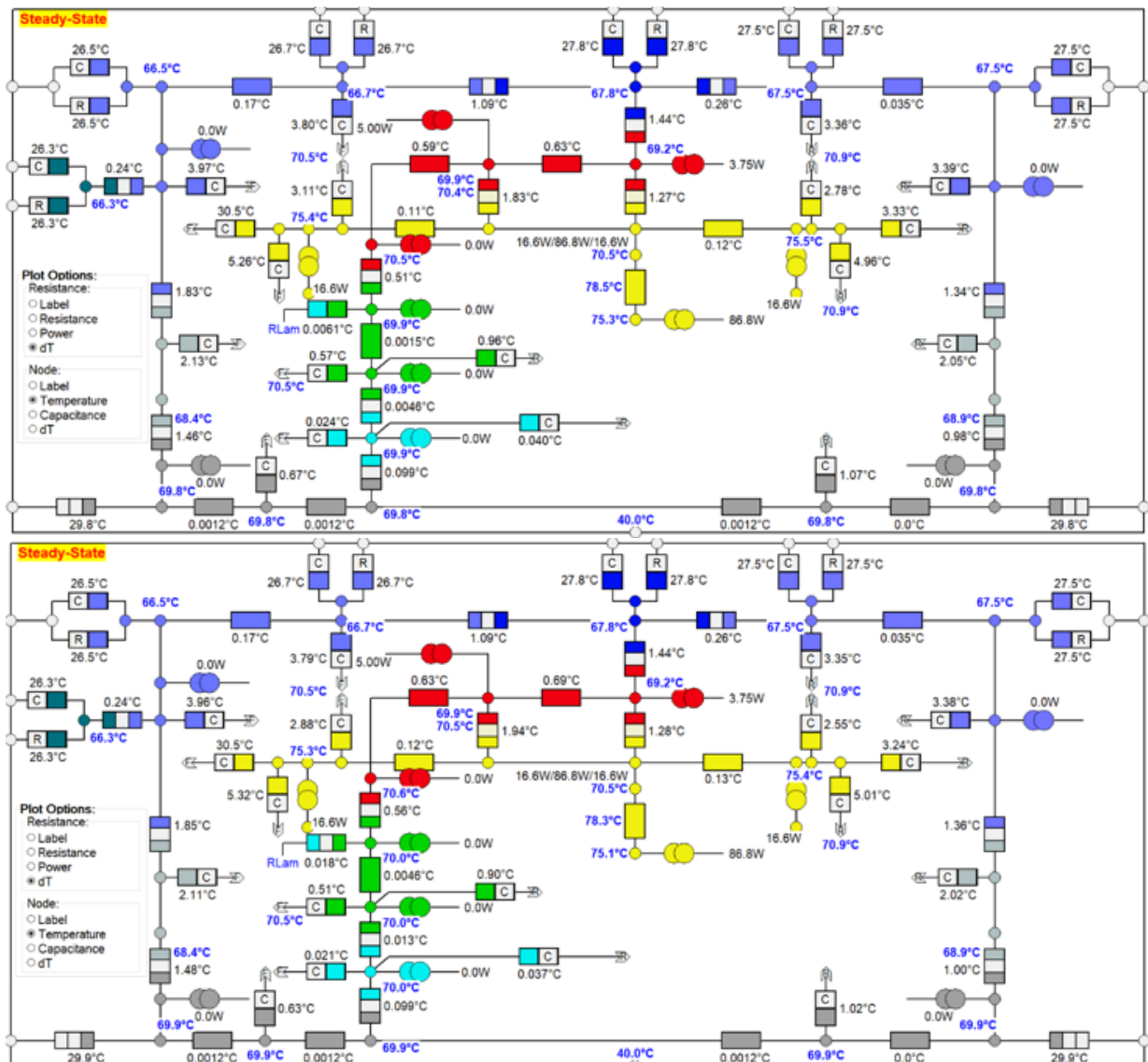


Figure 10. Thermal circuit equivalent of inset PMSM (top) and SPMSM (bottom)

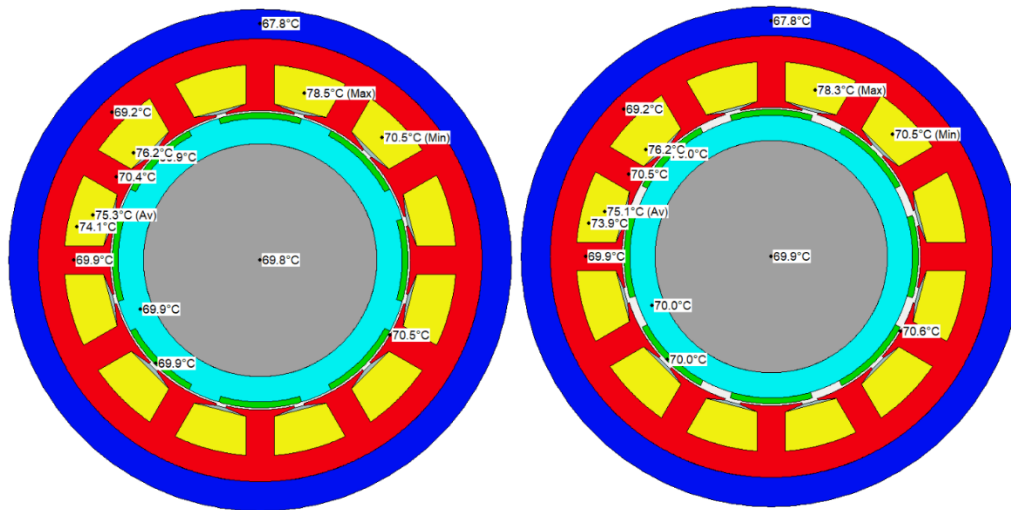


Figure 11. Temperature rise of inset SPMSM (left) and SPMSM (right)

This suggests that heat loss in the PMs of the inset PMSM is greater than in the SPMSM. The increased heat loss in the inset PMSM is attributed to the positioning of its PMs, which are embedded within the rotor. This design makes it more difficult to dissipate heat effectively, presenting a significant challenge for this type of machine.

Table 4. Temperature rise

Position	SPMSM (°C)	Inset PMSM (°C)
Shaft	69.9	69.8
Teeth	70.5	70.4
Slot	78.3	78.5
Rotor yoke	70	69.9
Stator yoke	69.2	69.2
PM	70	69.9

5. CONCLUSIONS

The paper has proposed the analytical model and FEM to evaluate two types of practical motors (SPMSM and inset PMSM) with a power rating of 7.5 kW. The obtained results from the proposed methods have analysed and compared the electromagnetic parameters of each motor, such as the magnetic flux density, cogging torque, torque ripple, flux linkage, electromagnetic torque, back EMF, and temperature rise. Based on the achieved results, the findings offer valuable insights into the strong and weak points of each motor type, aiding researchers and designers in selecting appropriate configurations, torque density, and efficiency for electric drives and industrial applications, and their impact on overall vehicle performance as well. Furthermore, this study lays the groundwork for future research to improve the electromagnetic parameters of these motors via the optimization techniques, including genetic algorithms, swarm optimization, and other advanced methods.

ACKNOWLEDGMENT

This research is funded by Hanoi University of Science and Technology (HUST) (Grant No.: T2024-PC-060).

REFERENCES

- [1] El-Kharashi, E. (2015). Approaches to prove the rotor of the permanent magnet machine must be outside in order to improve the energy conversion process. *International Journal of Applied Electromagnetics and Mechanics*, 47(1): 141-152. <https://doi.org/10.3233/JAE-140003>
- [2] Wang, Z.G., Gong, J.Y., Liu, B. (2023). Multi-objective optimization of the hollow shaft direct drive motor. *Advances in Mechanical Engineering*, 15(3): 16878132231163079. <https://doi.org/10.1177/16878132231163079>
- [3] Jusoh, L.I., Sulaiman, E., Bahrim, F.S., Kumar, R. (2017). Design comparison of inner and outer rotor of permanent magnet flux switching machine for electric bicycle application. *IOP Conference Series: Materials Science and Engineering*, 226(1): 012129. <https://doi.org/10.1088/1757-899X/226/1/012129>
- [4] Jung, W.S., Lee, H.K., Lee, Y.K., Kim, S.M., Lee, J.I., Choi, J.Y. (2023). Analysis and comparison of permanent magnet synchronous motors according to rotor type under the same design specifications. *Energies*, 16(3): 1306. <https://doi.org/10.3390/en16031306>
- [5] Choi, J.Y., Park, H.I., Jang, S.M., Lee, S.H. (2011). Design and analysis of surface-mounted PM motor of compressor for electric vehicles applications according to slot/pole combinations. *The Transactions of the Korean Institute of Electrical Engineers*, 60(10): 1846-1857. <https://doi.org/10.5370/KIEE.2011.60.10.1846>
- [6] Murakami, H., Honda, Y., Kiriya, H., Morimoto, S., Takeda, Y. (1999). The performance comparison of SPMSM, IPMSM and SynRM in use as air-conditioning compressor. In *Conference Record of the 1999 IEEE Industry Applications Conference. Thirty-Forth IAS Annual Meeting (Cat. No.99CH36370)*, Phoenix, AZ, USA, pp. 840-845. <https://doi.org/10.1109/IAS.1999.801607>
- [7] Cho, S.K., Jung, K.H., Choi, J.Y. (2018). Design optimization of interior permanent magnet synchronous motor for electric compressors of air-conditioning systems mounted on EVs and HEVs. *IEEE Transactions on Magnetics*, 54(11): 1-5. <https://doi.org/10.1109/TMAG.2018.2849078>

- [8] Zhu, Z.Q., Howe, D. (2000). Influence of design parameters on cogging torque in permanent magnet machines. *IEEE Transactions on energy conversion*, 15(4): 407-412. <https://doi.org/10.1109/60.900501>
- [9] Zhang, P., Sizov, G.Y., Demerdash, N.A. (2011). Comparison of torque ripple minimization control techniques in Surface-Mounted Permanent Magnet Synchronous Machines. In 2011 IEEE International Electric Machines & Drives Conference (IEMDC), Niagara Falls, ON, Canada, pp. 188-193. <https://doi.org/10.1109/IEMDC.2011.5994641>
- [10] Feng, L., Yu, S., Zhang, F., Jin, S., Sun, Y. (2022). Study on performance of low-speed high-torque permanent magnet synchronous motor with dynamic eccentricity rotor. *Energy Reports*, 8: 1421-1428. <https://doi.org/10.1016/j.egyr.2022.03.018>
- [11] Kim, S.J., Park, E.J., Jung, S.Y., Kim, Y.J. (2017). Transfer torque performance comparison in coaxial magnetic gears with different flux-modulator shapes. *IEEE Transactions on Magnetics*, 53(6): 1-4. <https://doi.org/10.1109/TMAG.2017.2663429>
- [12] Dong, J.N., Huang, Y.K., Jin, L., Lin, H.Y. (2016). Comparative study of surface-mounted and interior permanent-magnet motors for high-speed applications. *IEEE Transactions on Applied Superconductivity*, 26(4): 1-4. <https://doi.org/10.1109/TASC.2016.2514342>
- [13] Du, G.H., Li, N.M., Zhou, Q.X., Gao, W.T., Wang, L., Pu, T. (2022). Multi-physics comparison of surface-mounted and interior permanent magnet synchronous motor for high-speed applications. *Machines*, 10(8): 700. <https://doi.org/10.3390/machines10080700>
- [14] Xia, Y., Li, J., Qu, R., Fang, H. (2016). Comparison of two rotor topologies for high-speed permanent magnet synchronous machines. In 2016 XXII International Conference on Electrical Machines (ICEM), Lausanne, Switzerland, pp. 1419-1425. <https://doi.org/10.1109/ICELMACH.2016.7732710>
- [15] Liu, X., Zhang, Z., Xiao, J., Xu, H. (2018). Comparison and analysis of electromagnetic characteristics of IPMSM with single and double layer PMs. *International Journal of Applied Electromagnetics and Mechanics*, 58(4): 483-496. <https://doi.org/10.3233/JAE-180032>
- [16] Arehpanahi, M., Kheiry, E. (2020). A new optimization of segmented interior permanent magnet synchronous motor based on increasing flux weakening range and output torque (research note). *International Journal of Engineering*, 33(6): 1122-1127. <https://doi.org/10.5829/ije.2020.33.06c.09>
- [17] Xuan, H.V. (2012). Modeling of exterior rotor permanent magnet machines with concentrated windings. Doctoral dissertation, Technische Universiteit Delft.
- [18] Ojaghi, M., Sabouri, M., Faiz, J., Ghorbanian, V. (2014). Exact modeling and simulation of saturated induction motors with broken rotor bars fault using winding function approach. *International Journal of Engineering*, 27(1): 69-78. <https://doi.org/10.5829/idosi.ije.2014.27.01a.10>
- [19] Sadarangani, C. (2006). Electrical machines-design and analysis of introduction and permanent magnet motors. <https://www.semanticscholar.org/paper/Electrical-Machines-Design-and-Analysis-of-and-Sadarangani/5ff4b11f21539fd80c8816d97e035982213b23eb>.
- [20] Roy, P. (2020). Thermal modeling of permanent magnet synchronous motors for electric vehicle application. Master's dissertation, University of Windsor.
- [21] Pu, T., Du, G., Tong, J., Huang, N., Li, N., Xu, W. (2021). Comparison of rotor strength of various rotor structures for ultra-high-speed permanent magnet synchronous motor. In 2021 IEEE 4th Student Conference on Electric Machines and Systems (SCEMS), Huzhou, China, pp. 1-6. <https://doi.org/10.1109/SCEMS52239.2021.9646110>
- [22] Sahebjam, M., Bannae Sharifian, M.B., Feyzi, M.R., Sabahi, M. (2019). Novel unified control method of induction and permanent magnet synchronous motors. *International Journal of Engineering*, 32(2): 256-269.
- [23] Dorrell, D.G., Hsieh, M.F., Popescu, M., Evans, L., Staton, D.A., Grout, V. (2010). A review of the design issues and techniques for radial-flux brushless surface and internal rare-earth permanent-magnet motors. *IEEE Transactions on Industrial Electronics*, 58(9): 3741-3757. <https://doi.org/10.1109/TIE.2010.2089940>
- [24] Conga, T.T., Vua, T.N., Minha, D.B., Thanhc, H.V., Quoc, V.D. (2024). Analytical modelling of a six-phase surface mounted permanent magnet synchronous motor. *International Journal of Engineering*, 37(7): 1274. <https://doi.org/10.5829/ije.2024.37.07a.07>